Theoretical and Applied Climatology
https://doi.org/10.1007/s00704-022-03922-y

ORIGINAL PAPER

The long-term (142 years) spatiotemporal reconstruction and synoptic analysis of extreme low temperatures (– 15 °C or lower) in the northwest region of Iran

Mehdi Aalijahan[1] · Anthony R. Lupo[2] · Bromand Salahi[1] · Yusef Ghavidel Rahimi[3] · Manuchehr Farajzadeh Asl[3]

Received: 17 May 2020 / Accepted: 30 December 2021

Abstract
The present research has been performed for the temporal-spatial reconstruction of an extreme cold episode (temperature anomaly – 15 °C) occurring over the northwest part of Iran for a 142-year period (1871–2012). In carrying out the following investigation, the NOAA Twentieth Century (V20) reanalysis data including mid-level and sea-surface-level data were used. In order to achieve the research goals and extract the sea-surface and mid-troposphere patterns, the methods of hierarchical clustering and factor analysis were utilized. The results showed that during the 142-year period, a total of 791 days were identified in which temperature of – 15 °C or lower occurred. For the synoptic analysis, 183 of these days during which the temperature anomaly was widely observed across the study area were used. The results demonstrated that for most of these days, a surface high pressure system over Asia Minor and northwest Iran contributed to extreme low temperature. These high-pressure systems, whether individually or as part of an extended episode of occurrences, affected the study area. Furthermore, the upper air level study demonstrated that the occurrence of atmospheric blocking or high latitude troughs located to the northwest of Iran (or upstream) and extending into the study area were the main causes for these low temperatures.

1 Introduction

The frequency of extreme temperature and precipitation are two aspects of climate that will be affected by the current change in climate, and society needs to be fully prepared for the consequences of these events as they affect populations, infrastructures, environment, agriculture, systems, and sectors (López-Díaz and Conde 2013; Aalijahan and Khosravichenar 2021) such as private enterprise and governmental. Climate change research has shown that the number of hot days and their associated heat waves has been enhanced, while the number of frosts, cold days, and cold periods has been diminished in different parts of the world (Beniston et al. 2007; Della-Marta et al. 2007a, 2007b; Golden et al. 2008; Founda and Giannakopoulos 2009). In fact, the past three decades (1983–2012) have been the warmest since 1850 (IPCC, 2014). A description of the processes leading to meteorological extreme events and the proper representation of these processes in climate models are essential elements for the evaluation of potential future changes in the occurrence of these events (Beniston et al. 2007; Cattiaux et al. 2012).

Climate warming has increased the intensity and frequency of extreme climate events around the world, and these are often unprecedented in the last few decades definitively but possibly out thousands of years (Abbas et al. 2018). At the regional scale, climate change has led also to considerable temperature increases (Shahid 2010; Mayowa et al. 2015; Ghasemi 2015; Abatan et al. 2016). Additionally, these regional changes have been associated with changes in temperature variability and occurrences of extreme temperatures (Song et al. 2014; Matiu et al. 2016). The consequences of these changes are particularly noticeable in sensitive or vulnerable ecosystems such as arid regions (Salguero-Gómez et al. 2012; Dutta and Chaudhuri 2015) where extreme temperatures are a common phenomenon.

Extreme temperature anomalies are of special interest due to the severe impacts on the environment and ecosystems, economy, and human life (impacts on society, morbidity and mortality, physical comfort, agriculture) and they have been studied extensively on the local, regional, and global scales

✉ Mehdi Aalijahan
mehdi_alijahan@yahoo.com

[1] Mohaghegh Ardabili University, Ardabil, Iran

[2] University of Missouri, Columbia, USA

[3] Tarbiat Modares University, Tehran, Iran

Published online: 06 January 2022

(Aguilar et al. 2005; Alexander et al. 2006; Easterling et al. 2000; Meehl and Tebaldi 2004; Whan et al. 2016; Schindler 1997; Cooney 2012; Harsant et al. 2013; Kebede et al. 2015).

During the last few decades, changes in the frequency of extreme temperatures have been identified in various regions of the world (Brown et al. 2008; You et al. 2011; Mika 2013; Monier and Gao 2015; Gao and Franzke 2017). On local and regional scales, the occurrence of more frequent warm and cold extremes is possible (Alexander et al. 2006; Brown et al. 2008). Detection and representation of changes in the frequency of extreme temperatures were considered a challenge on the local and regional scales (Horton et al. 2015). In the recent past, increases in extreme cold temperatures have been observed in various parts of the world (Takahashi 1990; Zhang et al. 1996; Prieto et al. 2002; Ryoo et al. 2005; Kyselý 2008; Cony and Hernandez 2008; Hankes and Walsh 2011; Radinović and Ćurić 2012; Peterson et al. 2013; Parey & Hoang 2015; Van Oldenborgh et al. 2015; Mo et al. 2016; Ceccherini et al. 2015).

The study of extreme low temperatures, the synoptic analysis, and the extraction of atmospheric circulation patterns which led to the cold temperatures has drawn the attention of atmospheric scientists worldwide (Tannehill 1928; Simmonds and Richter 2000; Domonkos et al. 2003; Prieto et al. 2004; Cassano et al. 2005; Cony et al. 2008; Unkašević and Tošić 2015; Anagnostopoulou et al. 2017; Ning and Bradley 2015; Aalijahan et al. 2019). However, similar studies of events occurring over Iran by researchers from this country have been performed less frequently. Nonetheless, there are a few recent examples that can be cited (Alijani and Houshyar 2008; Lashkari 2008; Masoudian and Darand 2011; Ghavidel-Rahimi 2011a, 2011b; Ahmadi and Ghavidel-Rahimi 2011; Karimi et al. 2012; Ghavidel-Rahimi et al. 2016).

An example of research carried out for the northwestern region of Iran (NW Iran) was conducted by Ghavidel-Rahimi (2009). Ghavidel-Rahimi (2009) considered the occurrence of extreme low temperature over Northwest Iran to result from the eight surface and seven mid-tropospheric (500 hPa) circulation patterns identified in Table 1.

The objective of this paper is to identify the occurrences of extreme low temperature defined as those with a minimum temperature of − 15 °C and lower over a period of 142 years for NW Iran. The current research has been carried out based on synoptic analysis and the extraction of atmospheric patterns that led to this phenomenon using the NOAA Twentieth-century data (V20) which have a resolution of 2° latitude and longitude. The methods described above and in Yarnal (1993) or Barry and Perry (2001) were used for the synoptic analysis. Due to the lack of long-term data availability in Iran, such extensive climatological research has never been performed for the occurrence of the extreme low temperatures. From this point of view, the present study can provide a comprehensive summary of the 142-year trend and variability for extreme low temperatures and their associated atmospheric patterns for NW Iran.

2 Data and methods

2.1 Data

The study area is located within a box bounded by the latitudes of 34° to 39° N and longitudes of 44° to 50° E encompassing NW Iran (Fig. 1). The dataset used for this study was provided through the Twentieth Century Reanalysis Data and these are available at the following website address: https://www.esrl.noaa.gov/psd/data/gridded/data.20thC_ReanV2.html. Compared to other reanalysis, NOAA's Twentieth Century Reanalysis Data are available for a longer period of record than most data sets and are of acceptable accuracy (e.g., Compo et al. 2013).

For the upper air data, the study uses the 500-hPa geopotential height (m), sea surface pressure (hPa), zonal, and meridional winds (m s^{-1}), the 2-m surface temperature data (°C), and the 500-hPa temperature data (°C). The data set encompasses the years 1871–2012, totaling 142 years. The data are available four times per day (0000, 0600, 1200, and 1800 UTC) with a spatial resolution of 2° in longitude and 2° in latitude. The data are available on 24 pressure levels ranging from 10 to 1000 hPa. Due to the lack of synoptic stations within Iran encompassing the entire time period, no data from synoptic and meteorological stations were used. However, only the 2-m data of minimum surface temperature and upper air data were necessary to identify, classify, and extract extreme low temperature with a minimum temperature of − 15 °C.

2.2 Methodology

In order to identify the occurrence of − 15 °C (or lower) temperature extremes during the 142-year study, the temperature data were first extracted by scripting in GRADS. The low temperatures were identified as departures from the 142-year mean. Then, in order to extract the associated patterns of sea surface pressure and 500-hPa geopotential height, the individual days associated with the low temperatures were identified and then converted to a number and classified (Table 1) using factor and clustering methods.

For the classification and extraction of sea surface pressure and geopotential heights of 500-hPa patterns, a variety of factor analysis and hierarchical clustering methods were tested. Ultimately, the varimax rotation factor analysis method for sea surface pressure and hierarchical clustering with Euclidean distance for geopotential height patterns was identified as the superior method and their

Table 1 The surface and mid-troposphere (500 hPa) patterns led to the occurrence of extreme low temperatures in NW Iran (based on Ghavidel-Rahimi 2009, and obtained results of this research)

Row	Surface pattern	Mid-troposphere pattern
1	Northern European pattern	Red sea trough pattern
2	Western high-pressure pattern	Western European trough pattern
3	Middle East high-pressure pattern (Zagros mountains)	Turkmenistan-Black Sea trough pattern
4	Asia Minor high-pressure pattern (Ararat mountains) with low pressure East Iran	Eastern Caspian Sea deep trough pattern
5	Siberian high-pressure pattern	Troughing between the Black and Mediterranean seas
6	Integrated high-pressure pattern 1. High pressures(Siberian, Northwest European, Western migratory, Asia Minor) and low pressure (North Russia) 2. High pressures (Siberian, West China, Western migratory) and low pressure(Scandinavian) 3. High pressures(Siberian, Central Asia, Asia Minor, Western migratory, West China) and low pressure (polar side) 4. High pressures (Siberian, Western migratory, Northern European, Central European) and low pressures (Northeast and East Iran) 5. High pressures (Western migratory and Asia Minor) 6. High pressures (Western migratory and West China) and low pressures (North Russia and Scandinavian) 7. High pressures (Siberian, Balkans) and low pressure (Kazakhstan)	Kazakhstan trough pattern
7	Sub-Polar high-pressure pattern	Northeast Iran trough pattern
8	Central Asian high-pressure pattern	East Turkey trough pattern
9	Northwest European high pressure pattern with Turkey, Northeast and east Iran, and Kazakhstan low pressure	Ridge between Northwest and Southwest Russia
10	Central European high pressure pattern with Kazakhstan low pressure	Poleward regions deep trough pattern
11	-	Ridge between poleward regions and central Europe
12	-	Northwest European deep trough pattern
13	-	Central and East European omega blocking and trough between South Russia and Syria
14	-	Southern European dipole-shaped blocking and deep trough between South Russia and North Red sea
15	-	Central and Eastern European blocking and trough between Northwest Iran and South Russia
16	-	Scandinavian and Eastern European blocking and Northern European trough
17	-	European and Mediterranean blocking and poleward deep trough from North Russia

results are presented here. In order to draw the map of extracted patterns, the average of each pattern was first calculated. Then, this was transferred to "Surfer" software, eventually was interpolated by kriging method, and the maps were drawn. After extraction and analysis of the patterns, a representative index day was selected from each sea surface pressure patterns. The synoptic analysis was carried out on these index days in order to identify the causes of extreme low temperatures.

3 Results

3.1 Statistical analysis

The results of the analysis after extracting days with a temperature of − 15 °C and lower are shown in Fig. 2. Within the time period of 142 years, 791 days were identified with a temperature of − 15 °C and cooler in NW Iran.

Fig. 1 Overview map of the study area

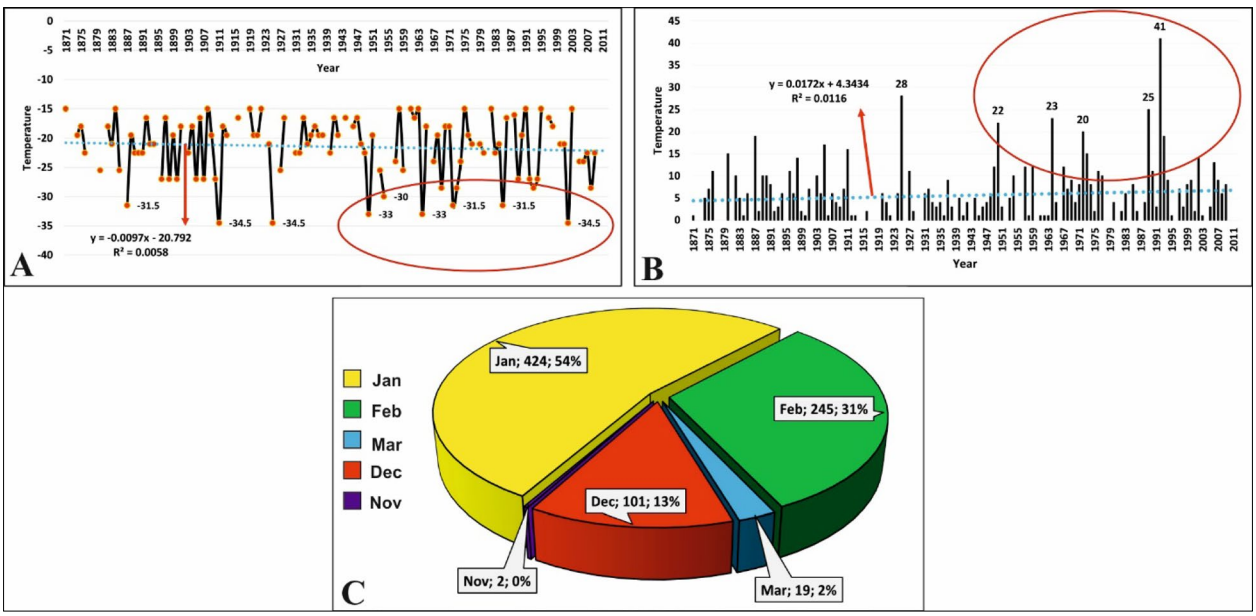

Fig. 2 **a** The time-series for the lowest yearly temperature (°C) occurring over the 142-period in NW Iran. **b** The annual occurrence (days) of − 15 °C temperature and lower over 142 years in NW Iran. **c** The number days and percentage of the monthly occurrence of − 15 °C and lower temperatures for NW Iran

Most of the low temperatures were identified during the months of November through March. In order of greatest monthly occurrence, these were January, February, December, March, and November at 424, 245, 101, 19, and 2 days, respectively (Fig. 2c). The most frequent annual occurrence was 41 days occurring in 1992. According

to Fig. 2b, the annual occurrence of low temperatures of − 15 °C and lower with a low coefficient of significance has increased since 1950. The lowest temperature recorded over the course of 142 years is − 34.5 °C, which occurred in three different years: 1911, 1925, and 2002. Examining Fig. 2a demonstrates that the severity of cold temperatures since about 1947 has increased as well. Thus, this region is witnessing the occurrence of more severe cold events.

3.2 Data validation

In order to validate the data used from synoptic stations in NW Iran, only the information provided by the Tabriz satiation was used due to the length and large volume of the data set (1951–2012) as well as the extraction method. The results of the validation of minimum temperature of Tabriz Station versus the minimum data from 2-m surface temperature from the Twentieth Century Reanalysis are shown in Fig. 3a and b. According to this figure, it can be shown that there is an acceptable correlation between the reanalysis data and the Tabriz station data either in terms of a time series or in terms of a scatter plot. The correlation value between the two data sets is 0.71 which is statistically significant at the 95% a confidence level.

3.3 Impacts of local factors

Apart from atmospheric factors affecting the occurrence of very low temperatures at global and regional levels in northwestern Iran, various local factors such as solar radiation, cloudiness, latitude, relief and topography, distance from seas and water bodies, and vegetation cover are also very effective. In the northwestern region of Iran, among the climate factors mentioned above, latitude and relief play the most important role in temperature distribution. However, the role of relief in the temperature distribution in this region and the occurrence of very low temperatures is much more obvious. The decrease in temperature with increasing elevation is very evident in the northwestern region of Iran. As can be seen from Fig. 1, the study area is strongly

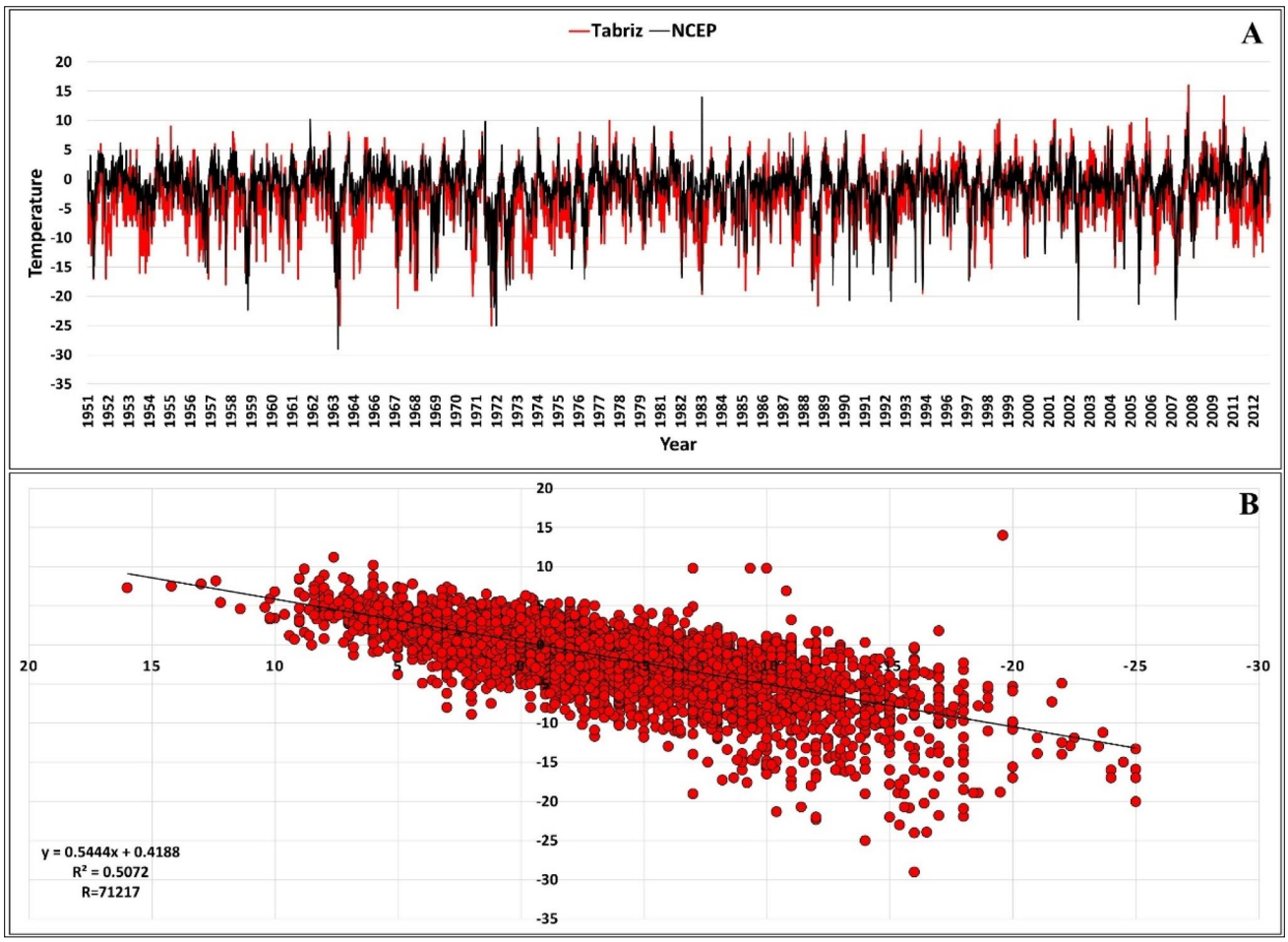

Fig. 3 **a** The comparative time series plot of minimum temperature (°C) recorded at the Tabriz synoptic station and NCEP data encompassing 1951 to 2012. **b** The scatter plot diagram and the correlation between the Tabriz ground station data and NCEP Twentieth Century Reanalysis

characterized by relief and is considered a complex mountainous region.

The minimum altitude of the area is 20 m, and the maximum altitude is 4811 m. On the other hand, the average altitude of synoptic stations in the region is over 1300 m. Low altitude areas are observed only in parts of the north of the study area near the Aras riverbed; therefore, the occurrence of very low temperatures in these areas is lower than in other parts.

Due to the very complex topography and high altitude in northwestern Iran, which have resulted in lower atmospheric thickness and thinner atmosphere, the thermal energy of outgoing longwave radiation can easily escape at night. On the other hand, the study area located between latitudes 34 and 39° N receives less solar energy during the cold season due to the inclination angle of radiation and shorter duration of radiation. This factor aggravates the occurrence of low temperatures as much as possible. The cooling of the air in these areas leads to the formation of local anticyclonic systems and causes the formation of air currents by creating a pressure gradient in relation to the low-lying areas (warm and low-pressure areas). On the other hand, when cold migrating air masses enter the northwestern region and combine with local high-pressure systems, this leads to very low temperatures locally in the areas affected by these air masses. From this point of view, the temperature difference between the NOAA organization data and the Tabriz station data (Fig. 3a, b) is due to the influence of local factors, especially the relief in the study area. In most cases, this temperature difference results in a lower minimum temperature being recorded at the Tabriz station than the temperature resulting from the NOAA organization data. This clearly shows the effect of local factors, especially relief, in exacerbating the occurrence of low temperatures.

Due to the lack of temporal coverage of the observation stations with long-term data, as well as the fact that the study of the role of local factors in the amplification and attenuation of the occurrence of very low temperatures in the study area is beyond the scope of this article and requires separate research, we refrain from further addressing this issue.

3.4 500-hPa geopotential height patterns

In order to identify the circulation patterns from the 500-hPa level, the surface temperature of − 15 °C or lower were extracted first for the study area. Then, by constructing a matrix with dimensions of 183 * 943 and utilizing an S-shaped array, a hierarchical cluster analysis method was used. These were clustered by Euclidean distance, and then the atmospheric patterns for NW Iran were extracted. As shown in Fig. 4, an 11-cluster classification system defined the circulation patterns using the 500-hPa level height

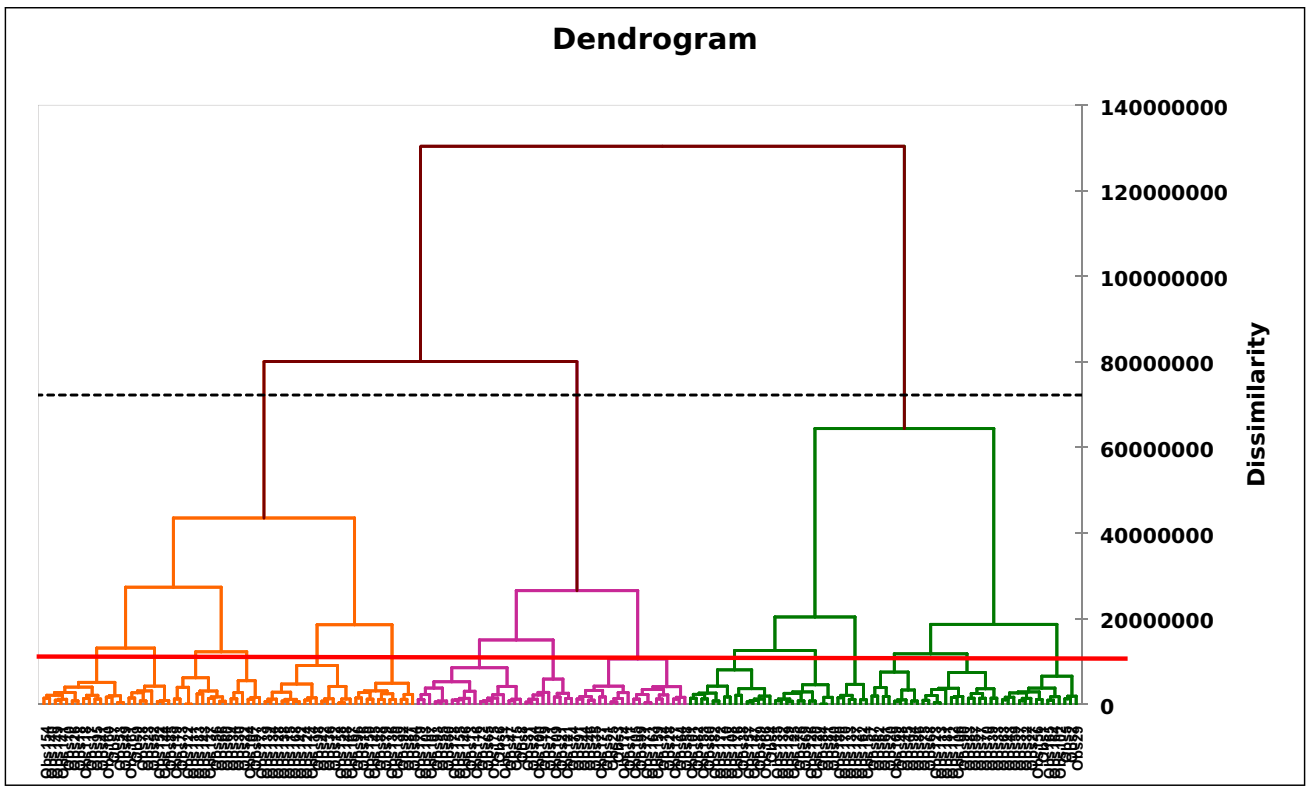

Fig. 4 The dendrogram for the 500-hPa patterns extracted from the geopotential height fields over NW Iran

Table 2 The number and percentage of days associated with the 11 patterns for 500-hPa geopotential height

Pattern	The number of days	Percent of pattern	Pattern	The number of days	Percent of pattern
1	23	12%	7	19	10%
2	14	8%	8	11	6%
3	6	3%	9	16	9%
4	26	14%	10	16	9%
5	20	11%	11	23	13%
6	9	5%			

associated with the surface temperature of − 15 °C and lower over NW Iran. The specification of the extracted patterns and the days associated with each pattern are shown in Table 4 in the Appendix and Table 2. They demonstrate that the most important contributors to the occurrence of very low temperature over the NW Iran region are pattern numbers 4, 11, 1, 5, 7, 9, 10, 2, 8, 6, and 3, respectively. The number of days associated with these patterns is 26, 23, 23, 20, 19, 16, 16, 14, 11, 9, and 6 days, respectively.

3.4.1 Pattern 1

This category comprised of 23 members with the coldest day at − 29 °C. For this atmospheric pattern, a trough exists over the eastern part of Turkey and the NW Iran region is located east of the trough and within a zone of cold air flux. It can be shown that the cold air is transported from latitudes poleward of 50° N from the Central European region into the region of NW Iran. The formation of this trough is responsible for the flow of cold air transported into northwestern Iran (Fig. 5a).

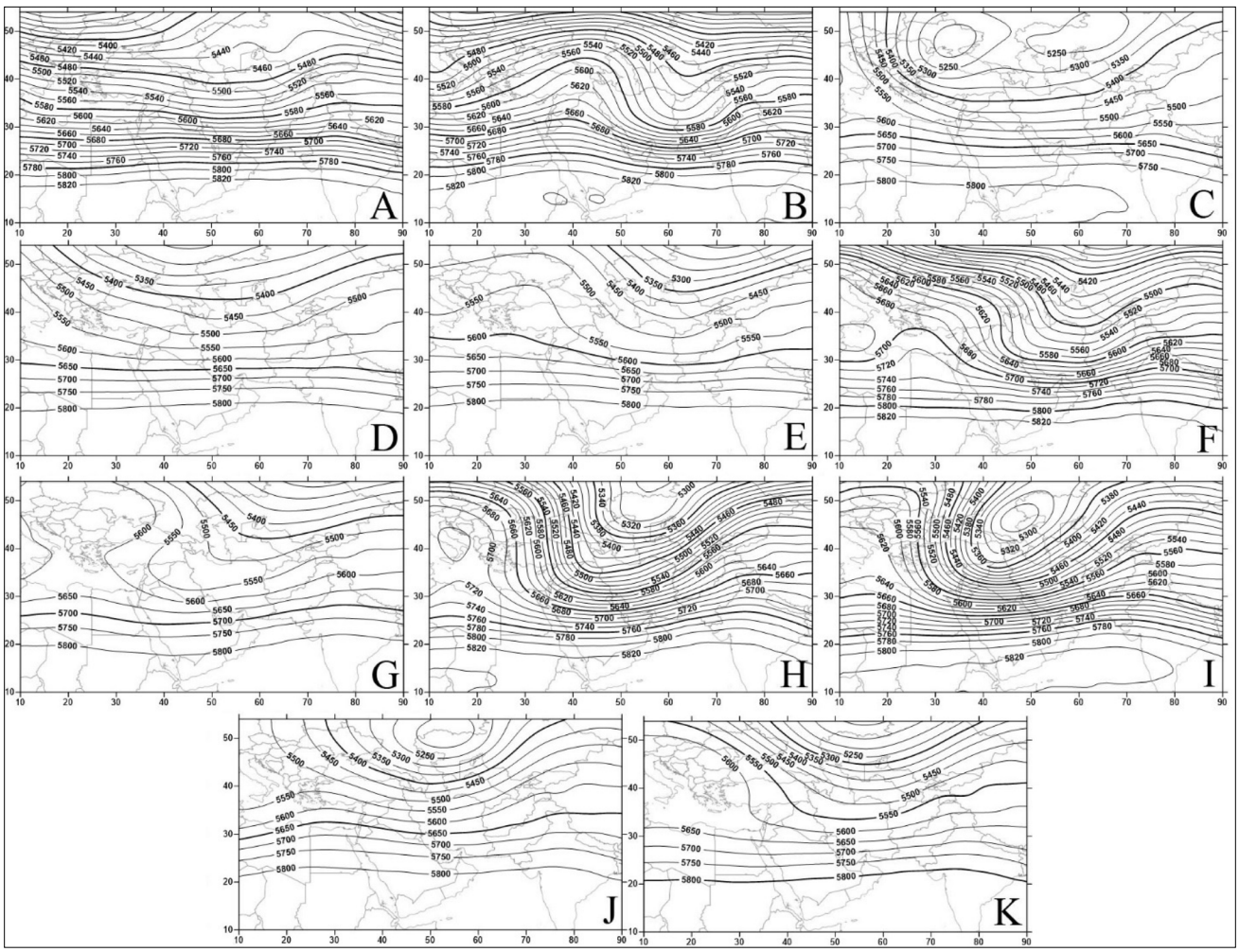

Fig. 5 The 500-hPa geopotential height patterns for (**a**) pattern 1, (**b**) pattern 2, (**c**) pattern 3, (**d**) pattern 4, (**e**) pattern 5, (**f**) pattern 6, (**g**) pattern 7, (**h**) pattern 8, (**i**) pattern 9, (**j**) pattern 10, and (**k**) pattern 11

3.4.2 Pattern 2

This atmospheric pattern consisted of 14 days. The temperature range for this respective pattern was − 10.5 °C, and the coldest day at − 28.5 °C, which occurred on 7 February 1950. The phenomenon observed in association with this pattern (Fig. 5b) is the occurrence of a ridge that spans the region from southwest Russia to northwestern Saudi Arabia. For this pattern, NW Iran is located exactly on the downstream flank of the ridge, where the maximum cold air transport or advection occurs.

3.4.3 Pattern 3

This cluster is associated with the occurrence of a particularly severe cold wave that persists for at least 6 days. Examining Fig. 5c shows the presence of two 500-hPa low pressure centers that are observed over Ukraine and Black Sea and to the northeast of the Caspian and Kazakhstan region. The low centers are embedded in a deep trough extending from latitudes poleward of 70° N, and also affecting the study area. The formation of this pattern is the result of an upstream blocking event and the change from zonal to meridional flow over Eastern Europe and Turkey. The respective trough carries cold air from northern Europe and the Russian region to the northern part of the country.

3.4.4 Pattern 4

This weather pattern, which consists of 26 days, is one of the coldest patterns at the 500-hPa geopotential height level. At the surface, the maximum cold intensity associated with this cluster was − 33 °C, which occurred on 16 January 1950. The pattern obtained from this cluster (Fig. 5d) represents a trough that was formed initially at latitudes north of 50° N and west of Europe and ultimately drawn east over the region of NW Iran. The formation of this pattern led to the direct transport of very cold weather from high latitudes to the study region.

3.4.5 Pattern 5

Figure 5e shows a map of 500-hPa geopotential height obtained for the 20 days that comprise of this cluster. The presence of a weak ridge extending poleward to latitudes higher than 55° N from central Europe to the location of northwestern Iran which is under the eastern part of the ridge is seen here (Fig. 5e). The formation of this pattern led to the flux of very cold air originating at latitudes poleward of 55° N to the region of NW Iran. It is noteworthy that the meridional nature of atmospheric flows over northern part of Iran contributes to the intensification and acceleration of cold air advection into the study region.

3.4.6 Pattern 6

The phenomenon that resulted in the formation of very cold air associated with this pattern was the occurrence of a deep trough extending from latitudes north of 60° N over northwest of Europe. The aforementioned trough has led to the formation of a weak ridge over the Russia, Azerbaijan, Armenia, Georgia, and Turkey, whose axis lies from southwest to northeast (Fig. 5f). For this pattern, the NW Iran lies within a downstream trough associated with strong height gradients and within a maximum of cold air advection. This mechanism is the cause of very cold air dominating over the mid-troposphere of the region (Fig. 5f).

3.4.7 Pattern 7

This atmospheric pattern consists of 19 days (Fig. 5g), and at 500-hPa height level is associated with an omega-shaped blocking event over central and eastern Europe and the location of NW Iran is in the southeast part of this block. Downstream of this block, a trough was located across southern Russia to parts of Turkey, Iraq, and Syria. As in pattern 6, the axis of this trough lies southwest to northeast which also crosses over NW Iran. The presence of this pattern is also associated with the occurrence of extreme low temperatures during the cold part of the year.

3.4.8 Pattern 8

The average 500-hPa geopotential height field associated with this pattern consists of about 11 days (Fig. 5h). The occurrence of a dipole-shaped blocking event over southern Europe, and also the formation of very deep trough with strong height gradients. The axis of this trough from the northern Red Sea to southern Russia is also evident in Fig. 5h and lies over NW Iran. Thus, the northwest part of the country lies under very strong cold air advection and the occurrence of extreme low temperatures in this region can be attributed to this pattern. The transport of cold air by blocking events (patterns 7 and 8) from latitudes north of 50° N west of Iran and 70° N north of Iran is a major cause of extreme low temperature occurrence in the region.

3.4.9 Pattern 9

The 16 days associated with this pattern reflect the occurrence of low amplitude blocking that was located over central and eastern Europe. A downstream trough extended from NW Iran to southwest Russia. This pattern is associated with strong northerly flow and is one of the coldest 500-hPa geopotential height configuration. According to Fig. 5i, there were 3 days in this cluster accompanied by temperature below − 30 °C and the absolute minimum

was – 33 °C. The low amplitude blocking and the deep downstream trough resulted in the strong transport of cold air from latitudes poleward of 70° N into the study region. Five persistent cold waves of four, three, and 2 days, respectively, are part of this cluster, which confirms the role of blocking in the occurrence of prolonged cold spells (e.g., Efe et al. 2020).

3.4.10 *Pattern 10*

As in pattern 9, there were 16 days that were clustered into this pattern. This pattern was associated with the absolute lowest temperature in NW Iran. The lowest surface temperature recorded in the northwest region was – 34.5 °C, occurring on 14 February 1911 under pattern 10. The temperature range of respective pattern is about – 18 °C, indicating a higher degree of cold weather in this cluster. The primary phenomenon associated with this pattern is a very deep low pressure center over western Kazakhstan and southwest Russia. This is associated with an upstream blocking event centered over Scandinavia and northern Europe and results in the transport of cold air into the study region from areas north of 70° N (Fig. 5j).

3.4.11 Pattern 11

This atmospheric pattern is one of the colder configurations for the study region and the lowest temperature recorded here was – 34 °C. This pattern (Fig. 5k) consisted of 23 members, and it was associated with a blocking ridge similar to pattern 10. However, this event was centered over Europe but extending to latitudes poleward of 60° N. Downstream of the ridge, a very deep trough was centered poleward of 60° N over northern Russia and extending equatorward to western Iran and lower latitudes. The blocking ridge over central Europe led to the transport of very cold air from northern latitudes to the east. In the downstream part of the ridge, cold air was advected into northwestern Iran, which was located near the axis of the deep trough, which is where the maximum cold air is accumulated (Fig. 5k).

3.5 Sea surface pressure patterns

The specification of surface patterns and the number of days associated with each is given in Table 5 in the Appendix and Table 3. These demonstrate that the main causes of the occurrence of extreme low temperature within NW Iran were patterns number 2, 1, 3, and 4, respectively. These four patterns accounted for 94% of the total surface pressure patterns associated with the coldest days in NW Iran.

Table 3 The percentage and number of days related to the sea surface pressure patterns

Pattern	The number of days	Percent of pattern	Pattern	The number of days	Percent of pattern
1	49	27%	6	4	2%
2	51	29%	7	1	0%
3	42	23%	8	1	0%
4	27	15%	9	2	1%
5	6	3%	10	1	0%

3.5.1 Pattern 1

This pattern of surface pressure over the northwestern region of Iran is one of the coldest patterns for surface pressure, and was associated with the second largest frequency of occurrence after pattern 2. This pattern was associated with the most severe low temperature days: – 34.5 °C occurring on 14 February 1911 and 27 January 1925. In this atmospheric pattern, four sea level pressure systems can be seen including the Siberian high, Northwest European high, Western migratory high (North Atlantic) and high pressure over Asia Minor, and a low-pressure system in northern Russia. The mechanism that affects NW Iran is the very cold air flow associated with the high pressures impacting the studied area, as well as the development of high pressure in Asia Minor. The role of the western migratory high pressure (originating over the North Atlantic) is the formation of a ridge over North Africa and southern Europe, the formation of a Mediterranean trough, and ultimately the transport of cold air from the direction of the Alps to the northernmost locations of the study region. On the other hand, low pressure located over Northern Russia also played a role in directing cold weather into northwest Iran. The result of this composite configuration was the occurrence of extreme cold events in the northwestern region of Iran (Fig. 6a).

3.6 Pattern 1—27 January 1925

The atmosphere over Eurasia was active on this day, and an intense high pressure that originally formed over northwest Europe and moved east towards the study area (Fig. 6b). The formation of a low pressure occurred over Russia and this was accompanied by the expansion of meridional flow towards the south. This migratory high pressure has led to the formation of packed gradient anticyclonic curvature over the northern and northeastern parts of Turkey. A high pressure reading of 1037.5 hPa is observed over the north part of Iran. At the 500-hPa level (Fig. 5i), the most evident phenomenon is a very deep trough extending from NW Iran to latitudes above 70° N. This trough was located downstream of a blocking event and split flow in the westerlies. This is

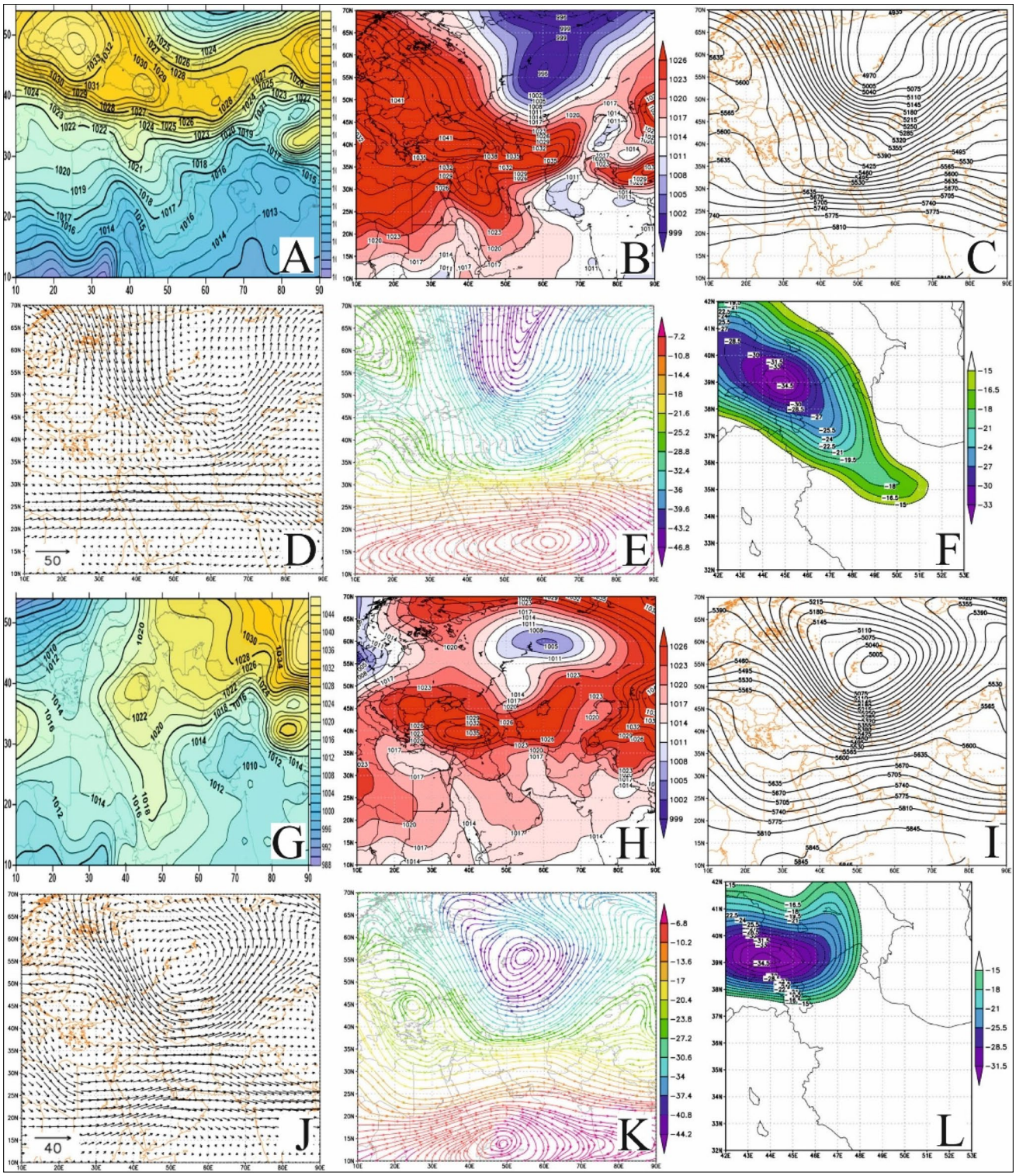

Fig. 6 The maps for patterns 1 and 2. Pattern 1 of (**a**) sea surface pressure (hPa), (**b**) sea surface pressure, (**c**) 500-hPa geopotential height (m), (**d**) wind at 500-hPa, (**e**) temperature advection at 500 hPa, (**f**) 2-m minimum temperature (°C). Pattern 2 of (**g**) sea surface pressure (hPa), (**h**) sea surface pressure, (**i**) 500-hPa geopotential height (m), (**j**) wind at 500 hPa, (**k**) temperature advection at 500 hPa, (**l**) 2-m minimum temperature (°C). For **b**, **c**, **d**, **e**, and **f**, the observation time is 0000 UTC 27 January 1925; and for **h**, **i**, **j**, **k**, and **l**, the observation time is 0000 UTC 27 December 2002

the main reason for meridional flow which aided the transmission of cold air from high latitudes into NW Iran. From 900 to 1000 hPa, gradually the geopotential height patterns became similar to the patterns of surface pressure. According to the temperature observations at 500–700 hPa, there was meridional flow from areas above 70° N directly into the study region. At 800–900 hPa, northerly flows along with divergence zones have formed above northern Turkey at the 950- and 1000-hPa levels. The Ararat Mountains over eastern part of Turkey play a major role in the flux of cold air into NW region of Iran. Examining Fig. 6f, it can be seen that the maximum cold occurrence over the northwestern corner of the country was − 34.5 °C.

3.6.1 Pattern 2

This surface pattern occurred most frequently in association with cold temperatures of − 15 °C and lower in the study region. The most severe cold day in this group occurred on 27 December 2002, with an average temperature of − 34.5 °C. According to the composite map for this pattern (Fig. 6g), a high-pressure system associated with the severe cold air over the NW region of Iran. This high pressure is a meridional extension of the Siberian high pressure from latitudes above 50° N to the northeast of the region. This high-pressure system leads to the formation and strengthening of the high-pressure region over Asia Minor including northwest Iran, Azerbaijan, Armenia, and eastern Turkey. The intensity of the Siberian high pressure as measured by central pressure in this pattern was 1044 hPa. The role of the Scandinavian low pressure, high pressure over western China, and a western migratory high pressure over the North Atlantic should not be ignored. The low pressures expand, and this leads to meridional flow over the central part of Fig. 6g aiding the transport of cold dry air from Siberia above 70° N into the study region.

3.7 Pattern 2—27 December 2002

The active surface pressure systems on this day are Siberian and Asia Minor high-pressure systems. According to Figs. 6h, i, and j, surface pressure, 500-hPa geopotential height, and wind flow are observed and the effect of high pressure that formed over eastern Turkey and NW Iran is more evident. The Siberian high pressure on this day entered from the east and combined with high pressure over Asia Minor. This mechanism contributed to the strength of the Asia Minor anticyclone. On the other hand, a cyclone has formed over central Russia and plays a role in strengthening the pressure gradients over the region. But this system is not only limited low levels. It was associated with a deep trough (Fig. 6i) extending from 35° N to 70° N. The signature of this trough can be seen up to the 800-hPa level over NW Iran. Thus, it can be shown that cold air is transmitted from latitudes poleward of 70° N into the study region from both the north and west. From the 850-hPa level upward, the effects of high pressure over eastern Turkey are clearly evident, indicating the intensity of the system. Up to 500-hPa level, the source region for the flux of cold air flow into NW Iran was poleward of 70° N and west of 55° E. From the 650–800-hPa layer, the source of cold air for the study region was from locations north and west of latitudes 50° N and 45° E over western Europe. But from the level of 850 to 1000 hPa, the cold air was accompanied by surface divergence over eastern Turkey, and this along with the funneling effect of the Ararat mountains plays a major role in the transmission of cold weather from the Ararat Mountain range into NW Iran (Fig. 6k). The intensity of the cold weather and its extent is quite evident in Fig. 6l.

3.7.1 Pattern 3

This pattern included 42 days from the total of 181 days reviewed. The lowest temperature achieved in NW Iran in association with this pattern is − 33 °C, which occurred on 16 January 1950. This composite pattern features a combination of a belt of high-pressure centers over Siberia, Central Asia, Asia Minor, and a western migratory high pressure over the North Atlantic. Within this pattern, the high-pressure system located over western Europe and the North Atlantic was accompanied by an average pressure of 1030 hPa, as well as a high pressure over Turkey with a central pressure of 1030 hPa. The high pressure over Turkmenistan and northeastern Iran had a central pressure of 1024 hPa, and the high pressure in western China has a central pressure of 1035 hPa. The combination of these pressure systems was accompanied by a polar side low pressure system that extends northward to latitudes above 50° N. The high-pressure systems, in particular the high-pressure system over Turkey, and the anticyclone to the west are accompanied by cold weather from western Europe and Alps Mountains. Combined with the central Asian high-pressure system led to the transport of very cold air flow from northerly latitudes into the surface of the studied area. The result of such a complex set of high-pressure systems is the domination and continuation of extremely cold weather in NW Iran (Fig. 7a).

3.8 Pattern 3—16 January 1950

The high-pressure systems that affected NW Iran on this day (Fig. 7b) include analogs for those shown in Fig. 7a. On the other hand, the polar low pressure was located over northern Europe near 70° N and expanded into Eastern Europe around 50° N. On this day, the study area is dominated by a 1020-hPa isobar. The high pressures that affect the NW

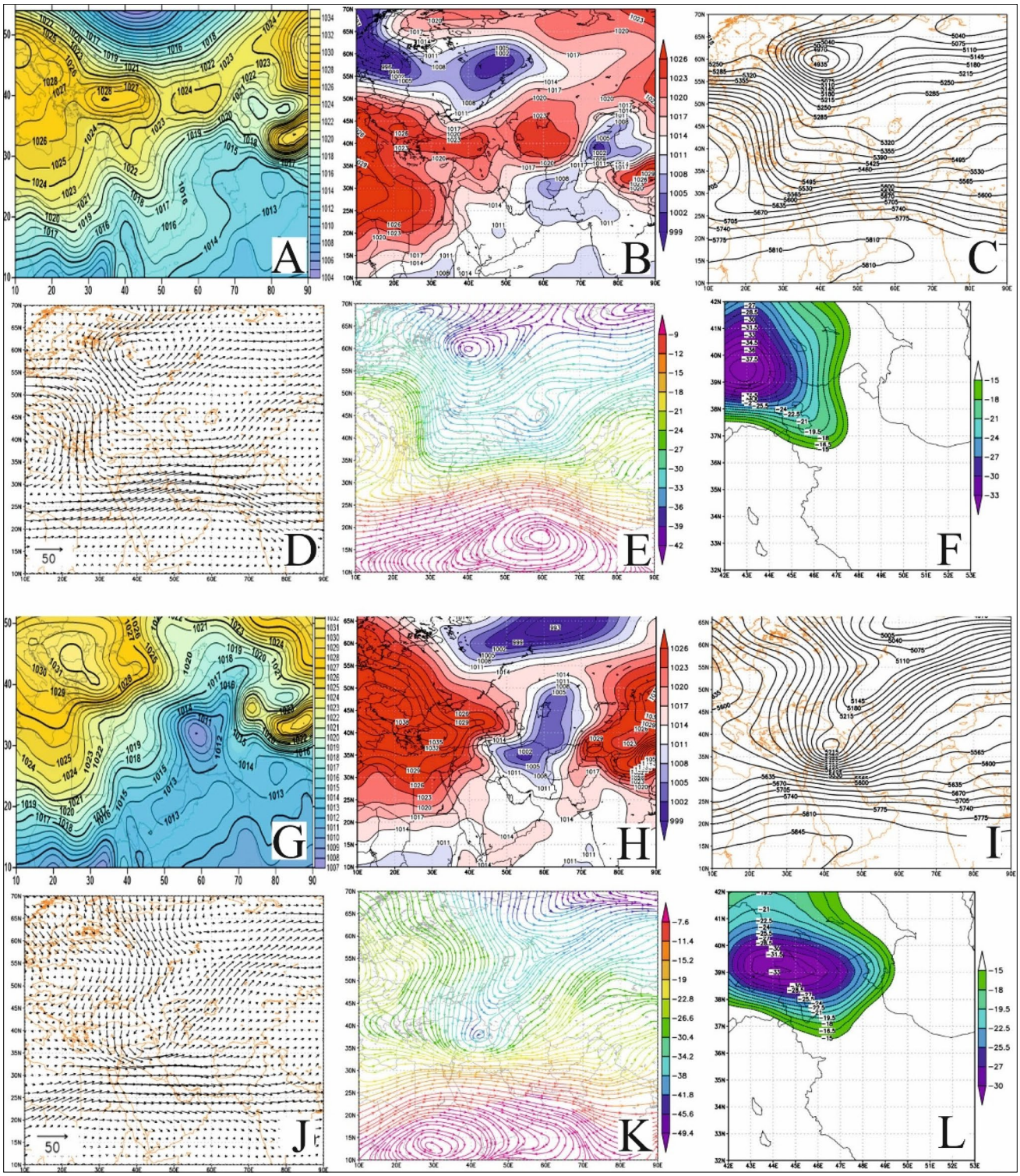

Fig. 7 The sea surface pressure pattern and the index day maps for patterns 3 and 4: pattern 3 of (**a**) sea surface pressure pattern (hPa), (**b**) sea surface pressure, (**c**) 500-hPa geopotential height (m), (**d**) wind at 500 hPa, (**e**) temperature advection at 500 hPa, (**f**) 2-m minimum temperature (°C); pattern 4 of (**g**) sea surface pressure pattern (hPa), (**h**) sea surface pressure, (**i**) 500-hPa geopotential height (m), (**j**) wind at 500 hPa, (**k**) temperature advection at 500 hPa, (**l**) 2-m minimum temperature (°C). For the index day maps of **b**, **c**, **d**, **e**, and **f**, the observation time is 0000 UTC 16 January 1950; and for the index day maps of **h**, **i**, **j**, **k**, and **l**, the observation time is 0000 UTC 19 January 1964

Iran region were mainly the western migratory and Asia Minor high-pressure systems. As in Fig. 7a, this led to the transport of cold air from the Alps and Ararat mountains into NW Iran. An analysis of geopotential heights and mid-level wind flow (Fig. 7c) indicates the presence of a trough over Turkey and its extension over the study region. The impact of this trough is evident also at the 850-hPa level. Cold air originally from latitudes above 55° N is transported towards NW Iran by this trough. From 900 to 1000 hPa, gradually the dominance of Asia Minor high pressure over NW Iran became clear (Fig. 7c).

The source of cold air transported into northwest Iran in the 500 to 850 hPa layer (Fig. 7e) is located poleward of 55° N and originated from the western migratory high pressure from the North Atlantic. At levels close to the surface, cold air transport and surface divergence over eastern Turkey were the main source of cold air into the region. As shown in Fig. 7f, the effects of the Asia Minor high pressure were evident. The coldest weather that occurred on this day was located over eastern Turkey at − 37.5 °C. The − 33 °C isotherm covered NW corner of Iran, and temperatures of − 15 °C and lower covered a large part of the northwest.

3.8.1 Pattern 4

The composite surface pressure pattern obtained from this cluster is shown in Fig. 7g. In this figure, the high-pressure systems that led to the occurrence of severe cold weather in the study region are the Siberian, western migratory from the North Atlas region, Northwest Europe, and eventually central European high-pressure systems. For this pattern, the Siberian high pressure expands towards the west, while high pressure over northwest Europe expands meridionally to the south and migrates eastward towards central European. During this time, the system strengthens as well. It should be noted, however, that this migratory high is associated with an upper air feature as well. During pattern 4 (Table 5), the domination of this high-pressure system over NW Iran is associated with severe cold, and six of the 27 days observe temperatures below − 30 °C. A striking feature of this pattern is the concurrent occurrence of a deep low-pressure system over northeast and east Iran between these two high-pressure systems. The result is very strong pressure gradients in an arc over northeast and northwest Iran. The result is the advection of cold air in association with strong winds from Siberia as well as from central Europe via the Alps and Ararat Mountains into the study region.

3.9 Pattern 4—19 January 1964

The map of surface pressure, 500 hPa geopotential heights, and winds is shown in Figs. 7h, i, and j. At first glance, two phenomena are apparent; the first is a low-pressure system over the countries of Central Asia and central and northeastern Iran, and the second is a large and strong high pressure over Western and Central Europe with a central core pressure of 1039.5 hPa. These two pressure systems impacted the study region in a manner similar to Fig. 7g, with a southeast to northwest oriented pressure gradient over NW Iran carrying cold air from latitudes poleward of 60° N. At the mid-levels of troposphere (Fig. 7i), blocking flow is the noticeable phenomena occurring over NW Iran, eastern Turkey, and northeast Syria. A trough, extending from latitudes above 70° N and in combination with blocking, is associated with meridional flow and the advection of very cold air into the region.

Examining the temperature map (Fig. 7k), the source of the cold air appears to be from the northwest and out of central Europe. The coldest air on this day occurred over the northwestern corner of the country, with a minimum temperature of − 33 °C. Temperatures of − 15 °C and lower have covered a large part of the northwestern region of the country, and this was associated with one of the worst winter days for this region in terms of impact on the population.

3.9.1 Pattern 5

This pattern (Fig. 8a) is associated with a surface high pressure over the NW region of Iran and minimum temperatures of − 20 °C and colder were recorded. With pattern 5, there are two systems influential for the occurrence of extreme temperatures in the study region. The dominant system is the high-pressure system over NW Iran, Turkey, Armenia, Georgia, and the eastern Black Sea and the average central pressure is 1034 hPa. The other is located to the southeast of this system and is a strong low pressure with an average central pressure less than 1005 hPa located over the eastern part of Iran. The low-pressure system is located mainly over Afghanistan, Pakistan, and Iran for the composited days. The incidence of this pressure pattern increased the intensity of the pressure gradient between the two pressure systems in the southwest to northeast direction in the study region and from southeast to northwest south of the region. The strong pressure gradients and circulation result in the advection of clod air into the study region from latitudes poleward of 50° N over the Asia Minor region (Fig. 8a).

3.10 Pattern 5—7 February 1950

On this day (Fig. 8b), two pressure systems were identified similar to the composite for pattern 5 and their centers were located over similar regions to Fig. 8a. The high-pressure region was located over NW Iran, and was associated with very cold, severe, and stable weather. The strong pressure gradients between these two systems resulted in the advection of very cold air from both Asia Minor and Ararat

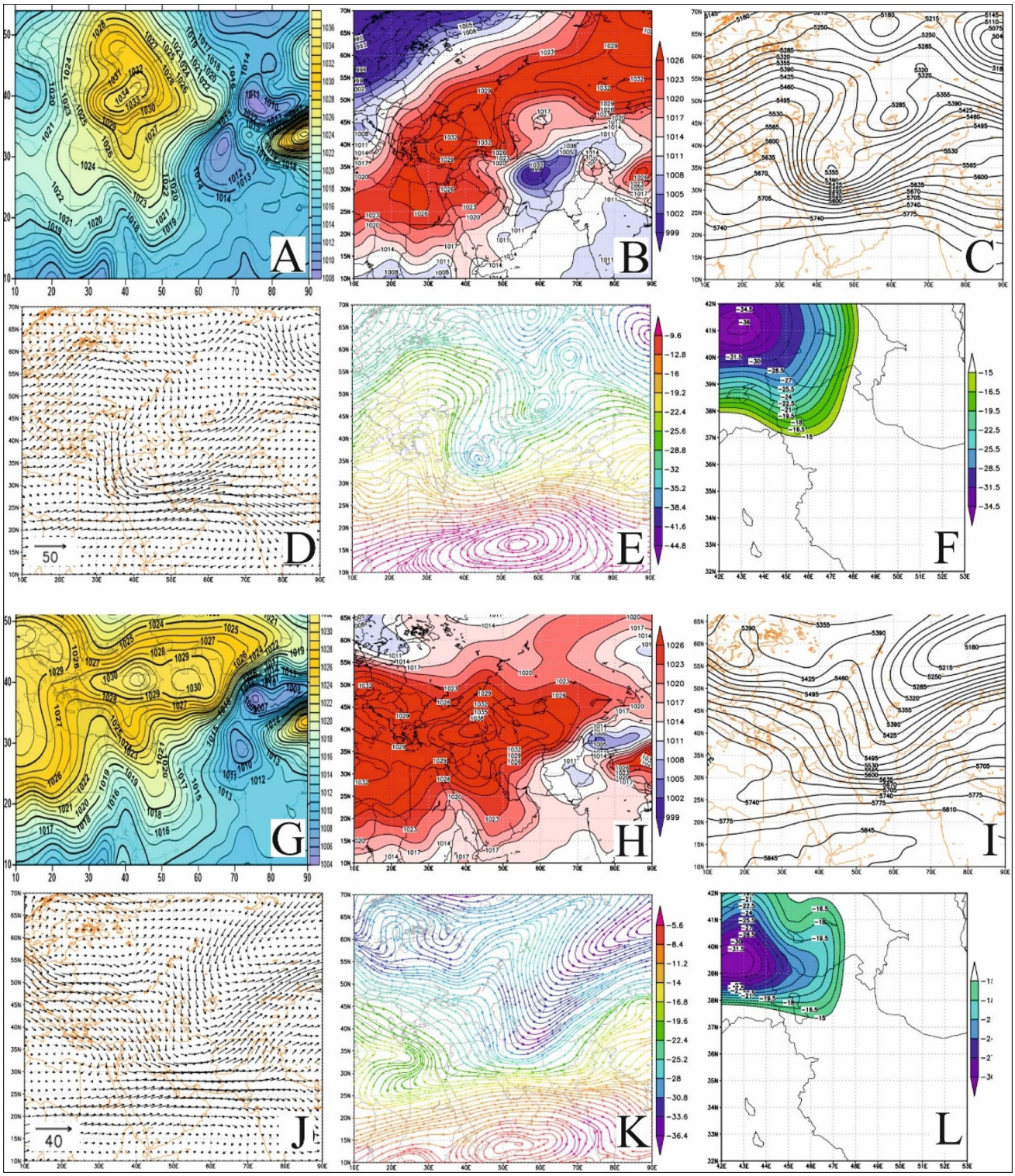

Fig. 8 The maps of synoptic analysis for patterns 5 and 6: pattern 5 of (**a**) the pattern of sea surface pressure in 142 years (hPa), (**b**) sea surface pressure, (**c**) 500-hPa geopotential height (m), (**d**) wind at 500 hPa, (**e**) temperature advection at 500 hPa, (**f**) 2-m minimum temperature (°C); pattern 6 of (**g**) the pattern of sea surface pressure in 142 years (hPa), (**h**) sea surface pressure, (**i**) 500-hPa geopotential height (m), (**j**) wind at 500 hPa, (**k**) temperature advection at 500 hPa, (**l**) 2-m minimum temperature (°C). For **b**, **c**, **d**, **e**, and **f** index day maps, the observation time is 0000 UTC 7 February 1950; and for **h**, **i**, **j**, **k**, and **l** index day maps, the observation time is 0000 UTC 7 December 1994

Mountains. In the mid-levels (Fig. 8c), a strong trough is evident over the western part of Iran. This trough is associated with the transport of cold air from latitudes poleward of 60° N. At the 800–950-hPa levels, the trough was active and played the role of carrying cold air from latitudes poleward of 55° N, including the southern part of Russia and Ukraine to the northwest.

The origin of cold weather on this day from the 500-hPa levels originates from the geographic latitudes poleward of 60° N which flows in a meridional direction towards the study region (Fig. 8e). At 850- and 900-hPa levels, the cold air was centered over northern Turkey. Finally, at the 950- and 1000-hPa levels, the eastern part of Caspian Sea supplied the cold weather and provided for clouds and snow over NW Iran similar to that which occurs downstream of the Great Lakes in the USA (not shown). On this day, the coldest air is located over northeastern Turkey, which has a temperature of − 36 °C and a − 28.5 °C contour was observed over NW Iran (Fig. 8f).

3.10.1 Pattern 6

Pattern 6 for NW Iran includes only 4 days out of the total of 181 days in which a temperature of − 15 °C or lower was observed. This pattern shows the presence of a western migratory anticyclone from over the North Atlantic and a high pressure over Asia Minor. The western anticyclone reinforces the central Asian anticyclone in transporting cold air into the study region. The combination of these systems leads to a cold air outbreak that stretches from has led to the domination of a high pressure in the northwest of the country, the concentration, and domination of the very cold air of central Europe and the Alps region all the way to Asia Minor. The Ararat mountains located near NW Iran may play a role in funneling cold air into the study region (Fig. 8g).

3.11 Pattern 6—7 December 1994

On 7 December 1994 (Fig. 8h), two high pressures are noted similar to those in Fig. 8g. The formation of the western migratory high pressure was responsible for transporting cold air out of Central Europe and the Alps Mountain region. This cold air moved into Turkey and combines with high pressure east of the Ararat Mountains to high pressure observed over the study region. In NW Iran, the 1035-, 1036.5-, and 1038-hPa contours associated with the Asia Minor high providing for very stable and cold weather. At the mid-levels, there was a very deep trough located at latitudes poleward of 50° N over Western Europe and extending to the other side of the Caspian Sea. This confirms that the source of the cold air is likely from Western Europe to the northwest. For the 850- to 1000-hPa levels, the geopotential height pattern is similar to the surface-pressure systems.

The source of cold air is from the northwest at 500 to 850 hPa, which originated from regions poleward of 50° N and passing through eastern Turkey. At the 850- to 1000-hPa level, NW Iran is strongly influenced by this cold air located over eastern Turkey. Examining the surface map (Fig. 8l), looking at the map, the minimum 2 m temperature of − 15 °C and lower influences a smaller area of the study region that the previous five patterns. The most severe cold recorded for eastern Turkey is − 31.5 °C, and the − 28.5 °C contour is observed over extreme NW Iran.

Due to those patterns 7, 8, 9, and 10 having occurred once or eventually twice in the study period and having not more impact on occurring low temperatures in the study area, for reducing the length of the manuscript, the analysis of the pattern of sea surface pressure has been just reflected.

3.11.1 Pattern 7

The pattern or cluster 7 included only one day, 30 January 1911, from the set of 181 days associated with temperatures of − 15 °C or lower within NW Iran. This day was not similar to any of the previous clusters. Figure 9a shows that this day was associated with three low-pressure centers and a high-pressure system over the western part of the country. This high-pressure system is detached from a larger migratory high pressure over northwest Europe, entering Iran from the west. This high pressure over the NW Iran region led to the transport of cold air from Northwest Europe. Additionally, the result of this pressure distribution is strong pressure gradients over Turkey and much of Iran.

3.11.2 Pattern 8

The pattern or cluster 8, like cluster 7, consists of only one day (17 January 2006). The surface pressure map for the study region is shown in Fig. 9b. On this day, there was a low-pressure system located over northeast Iran and the Caspian Sea. Also, a high-pressure system was located over central Europe originated from latitudes poleward of 70° N. Additionally, high pressure is noted over northeast Iran, with a central pressure of greater than 1020 hPa. On this day, three isobars (1018, 1020, and 1022 hPa) were located within the territory of NW Iran. Even though the surface pressure pattern is different, the result of this system is the advection of very cold air from northerly latitudes into NW Iran.

3.11.3 Pattern 9

For the cluster 9 (Fig. 9c), there were only two days out of 181 days. The NW region of Iran was influenced by a series

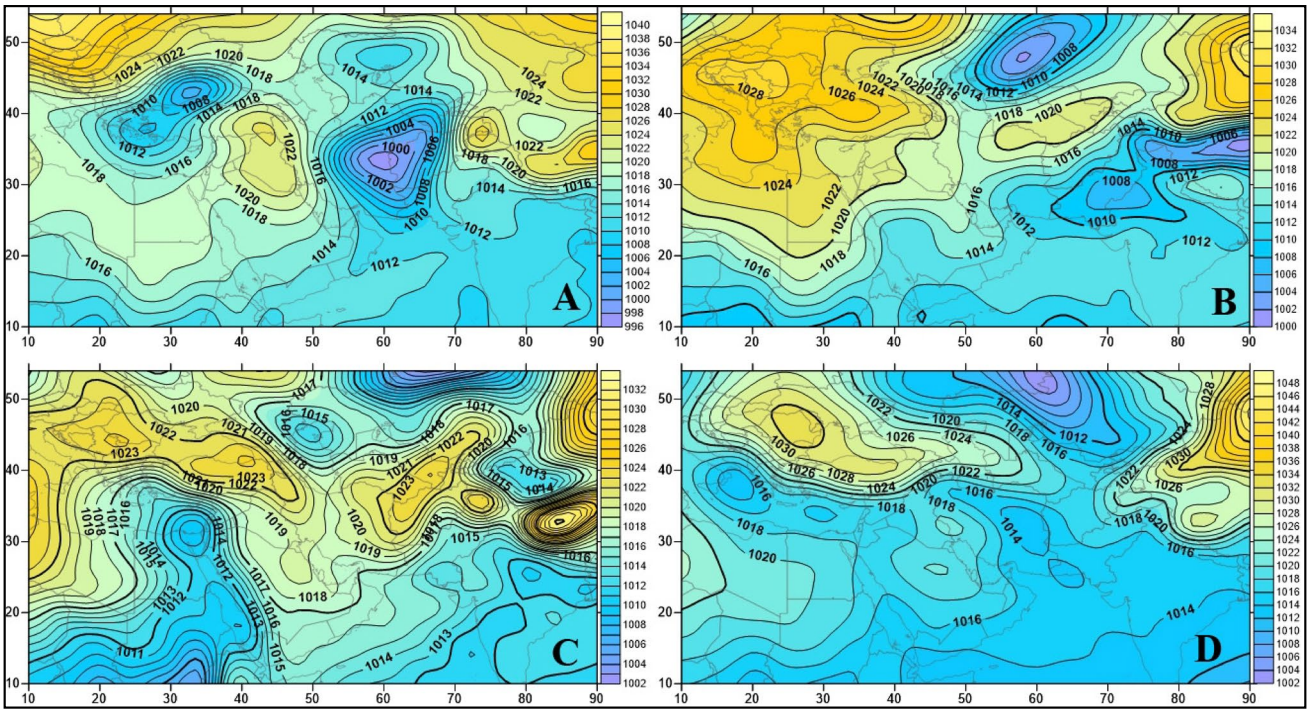

Fig. 9 The sea surface pressure patterns for (**a**) pattern 7, (**b**) pattern 8, (**c**) pattern 9, and (**d**) pattern 10

of high-pressure systems and a deep low pressure to the west of the region and another that was over the Caspian Sea, western China, and the northeastern region of Iran, Afghanistan, and Turkmenistan. On the left edge of Fig. 9c, a western migratory high pressure was present over southeastern Europe. Also, a strong pressure gradient is noted from central Europe to southeast Europe, eastern Turkey, Armenia, Georgia, and NW Iran. Additionally, a high pressure exists over western China, and smaller "lobes" are present over northeastern and eastern Iran. The presence of low pressure over the northern Caspian Sea leads to the existence of a strong pressure gradient oriented from northwest to southeast, indicating the transport of very cold air from northern and western Europe as well as from Central Asia, and Asia Minor into NW Iran.

3.11.4 Pattern 10

The final category, pattern 10 (Fig. 9d), included only one day (December 26, 2002). The minimum temperature found over NW Iran on this day was − 31.5 °C. In Fig. 9d, the Siberian high encompassed the far-right side of the map region-far-right side of the map region including western China. There was also a high-pressure system over the Balkans, as well as a deep low-pressure system over Kazakhstan. The pressure gradient created between the high pressure over the Balkans and central Asia was oriented from northwest to southeast in a similar manner to pattern 9. This is responsible for the transport of the very cold air over the western and inner part of Iran.

4 Discussion and conclusion

Based on the results of clustering and factor analysis methods for weather patterns impacting NW Iran, 11 upper air and 10 surface pressure patterns were extracted. Different combinations of surface high and low-pressure systems are responsible for transporting the very low temperature into the study region and these are named in Table 1. These patterns are associated with the occurrence of surface temperatures of − 15 °C or lower into the region. The area of origin and approximate direction of transport of these pressure systems are shown and summarized in Fig. 10.

In the mid-troposphere, there was a trough that extended into NW Iran from latitudes above 50° to 70° N, and from the regions of western and northwest Europe and Arctic regions. Some cold events were associated with deep troughs observed over central Asia mainly

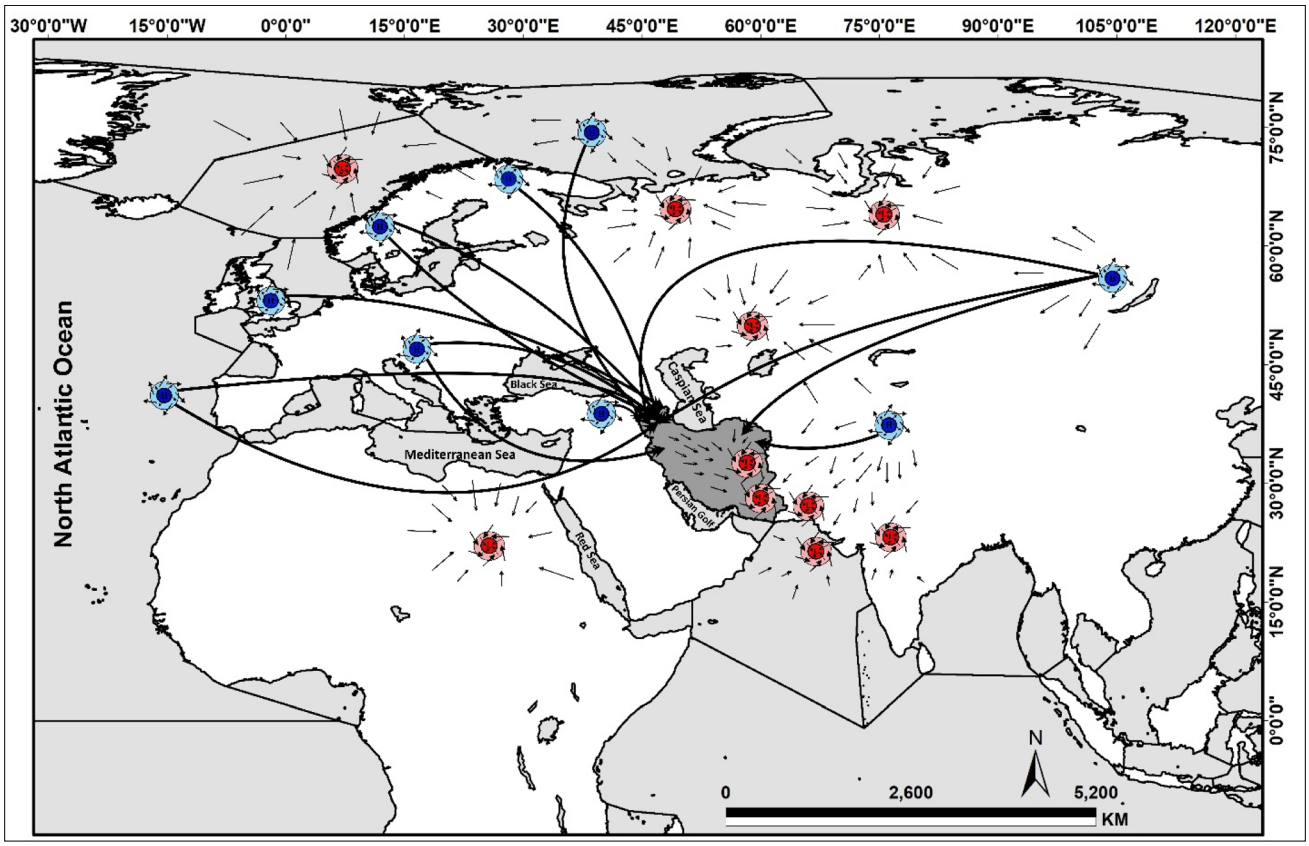

Fig. 10 The map of the formation regions and transport of cyclones and anticyclones associated with the occurrence of very low temperatures (− 15 °C and lower) in NW Iran

southern Russia and the Caspian Sea, as well as NW Iran, and southern Russia and northeastern Iran. According to these results, the occurrence of extremely low temperatures for NW Iran was associated with combinations surface pressure systems atmospheric blocking events, and upper air troughs and ridges.

The occurrence of very strong surface high pressures over central Asia had the greatest impact leading to the very coldest of these extreme cold air outbreaks. Additionally, the role of low pressures over the eastern, northeastern, and central regions of Iran and Central Asia also played a significant role in the transport or advection of cold air into the study region. These low pressures had the effect of helping to strengthen the pressure gradients over the region which in turn enhanced the transport of cold air into the northwest and internal part of Iran. In the mid-troposphere, atmospheric blocking located to the west of NW Iran were a major contributor to cold air outbreaks and these events were often the most persistent.

These results confirm previous studies in some cases and extends the results of others. The studies of extreme cold over NW Iran (e.g., Alijani and Houshyar 2008; Ghavidel-Rahimi 2011a, 2011b, 2009) emphasized the role of individual high-pressure systems in generating these conditions. According to the results obtained here, the cold air is often the result of deep high pressures at the surface that were the most effective reasons in the occurrence of these temperatures. In the mid-levels of the troposphere, the role of atmospheric blockings is very clear, which is similar to the results of Lupo et al. (2001), Nunes et al. (2017), and Efe et al. (2020) and others for different parts of the world. Additionally, this work showed the contribution of low pressures in a manner similar to cold air outbreaks over South America (e.g., Lupo et al. 2001).

Appendix

Table 4 The number of days for minimum temperatures less than − 15° C belonging to the eleven 500-hPa geopotential patterns over NW Iran

P	Day	T.Min	P	Day	T.Min	P	Day	T.Min	P	Day	T.Min
P1	15feb2005	− 22.5	P4	17feb1927	− 24	P7	19jan1993	− 22.5	P9	10feb1992	− 25.5
	14jan1885	− 22.5		31jan1950	− 19.5		15jan1993	− 27		9feb1992	− 27
	14feb2005	− 24		22feb1959	− 19.5		22feb1959	− 25.5		5feb1950	− 27
	6feb1974	− 21		21feb1959	− 25.5		6feb1989	− 21		29dec1924	− 21
	30jan1907	− 22.5		31dec1905	− 22.5		23feb1897	− 16.5		27jan1992	− 23.5
	11jan1977	− 19.5		9jan1909	− 19.5		16feb1950	− 24		30dec1924	− 19.5
	10jan1977	− 21		29dec1905	− 21		4feb1989	− 19.5	P10	22jan2006	− 22.5
	19feb1927	− 21		28dec1905	− 22.5		4jan1973	− 22.5		16feb1887	− 24
	18feb1927	− 24		18jan1950	− 22.5		5jan1964	− 19.5		23feb1985	− 31.5
	16jan1910	− 22.5		30dec1905	− 24		5jan1973	− 21		22feb1985	− 21
	15jan1910	− 22.5		3feb1989	− 21		11jan1964	− 21		31jan2006	− 24
	23jan1894	− 22.5		25jan1964	− 22.5		11mar1992	− 24		27jan1921	− 19.5
	22jan1894	− 16.5		25jan1903	− 21		12mar1992	− 25.5		26dec2002	− 31.5
	31jan1920	− 15		24jan1964	− 25.5		14jan2008	− 22.5		13feb1911	− 31.5
	22jan1890	− 22.5		23jan1964	− 25.5		15jan2008	− 24		15feb1911	− 28.5
	20jan1984	− 15		16jan1950	− 33		18jan2008	− 15		14feb1911	− 34.5
	18jan1954	− 21		15jan1950	− 21		20jan1925	− 18		9dec1927	− 24
	17jan1973	− 21		24dec1905	− 27		21feb1949	− 21		8dec1927	− 25.5
	13feb2005	− 21		23dec1905	− 27		22jan1957	− 24		6jan1942	− 21
	15jan1954	− 29		17jan1993	− 27		25dec1972	− 24		20jan1950	− 16.5
	16jan1954	− 25.5		17feb1993	− 24		27jan1992	− 22		19jan1950	− 19.5
	9jan1977	− 18		9jan1989	− 24		28jan1992	− 24		30jan1964	− 28.5
P2	8jan1977	− 16.5		30jan1950	− 19.5		31dec1889	− 21	P11	4jan1891	− 22.5
	14jan1910	− 22.5	P5	18jan1973	− 25.5		31jan1876	− 21		4jan1989	− 25.5
	10jan1909	− 19.5		10jan1935	− 16.5		31jan1887	− 22.5		5feb1907	− 24
	13jan1910	− 27		11jan1935	− 18	P8	6dec1994	− 25.5		6feb1887	− 22.5
	9feb2000	− 22.5		9feb1887	− 25.5		19jan1898	− 27		6feb1896	− 22.5
	8feb1950	− 24		31dec1948	− 21		28feb1959	− 21		6jan1964	− 19.5
	7feb1950	− 28.5		12jan1910	− 25.5		27jan1983	− 21		7feb1896	− 18
	28jan2001	− 18		7feb1880	− 21		18jan1898	− 21		10feb1896	− 19.5
	1feb1980	− 22.5		3feb1876	− 21		16jan2008	− 25.5		11jan1990	− 19.5
	29jan1946	− 18		30jan1974	− 22.5		26dec1931	− 22.5		12jan1964	− 19.5
	29jan1934	− 19.5		5feb1907	− 24		25dec1931	− 22.5		12jan1990	− 19.5
	20feb1994	− 18		20jan1973	− 16.5		18jan1993	− 16.5		16jan2006	− 21
	2feb1969	− 25.5		19jan1973	− 27		18feb1950	− 21		17jan2006	− 21
	4feb1969	− 24		30jan1925	− 22.5		12jan2009	− 22.5		19feb1950	− 24
	7jan1942	− 19.5		29jan1925	− 25.5	P9	25jan1925	− 27		22jan1993	− 22.5
P3	31jan1911	− 16.5		29dec2002	− 24		26jan1925	− 31.5		27dec1931	− 16.5
	30jan1911	− 25.5		5jan1972	− 24		24jan1925	− 22.5		27dec2002	− 34.5
	25jan1911	− 27		7jan1885	− 25.5		26jan1887	− 27		27jan1925	− 34.5
	24jan1911	− 27		22jan1964	− 24		22jan1925	− 18		28dec2002	− 31.5
	29jan1911	− 30		14jan1964	− 21		30jan1887	− 22.5		28jan1925	− 28.5
	28jan1911	− 21		13jan1901	− 15		27jan1887	− 31.5		28jan1983	− 21
P4	20feb1959	− 16.5	P6	8dec1994	− 24		23jan1911	− 24		29dec2006	− 22.5
	17jan1950	− 31.5		7dec1994	− 28.5		22jan1911	− 19.5		19jan1896	− 19.5
	28jan1950	− 19.5		6feb1957	− 21		19jan1964	− 33		19feb1950	− 24

Table 5 The number of days belonging to sea surface pressure patterns with minimum temperatures less than − 15 °C in the study area

P	Day	T.Min	P	Day	T.Min	P	Day	T.Min	P	Day	T.Min
P1	3feb1989	− 21	P1	31jan1887	− 22.5	P2	28dec2002	− 31.5	P3	29dec1905	− 21
	3feb1876	− 21		31jan1911	− 16.5		28jan2001	− 18		29dec2006	− 22.5
	4feb1989	− 19.5		31jan1950	− 19.5		29dec2002	− 24		29jan1925	− 25.5
	4jan1973	− 22.5	P2	31dec1905	− 22.5		29jan1934	− 19.5		31jan2006	− 24
	4jan1891	− 22.5		31jan1920	− 15		30dec1905	− 24	P4	5feb1950	− 27
	5feb1907	− 24		1feb1980	− 22.5		30dec1924	− 19.5		8jan1977	− 16.5
	5jan1964	− 19.5		2feb1969	− 25.5		30jan1907	− 22.5		9feb1992	− 27
	5jan1972	− 24		4feb1969	− 24		30jan1964	− 28.5		10feb1992	− 25.5
	5jan1973	− 21		6feb1974	− 21	P3	4jan1989	− 25.5		12jan1910	− 25.5
	6feb1989	− 21		7jan1942	− 19.5		5feb1907	− 24		13feb1911	− 31.5
	6jan1964	− 19.5		8feb1950	− 24		6feb1887	− 22.5		16jan2008	− 25.5
	7feb1880	− 21		9feb2000	− 22.5		6feb1896	− 22.5		18jan1898	− 21
	7jan1885	− 25.5		9jan1909	− 19.5		6feb1957	− 21		19jan1964	− 33
	8dec1927	− 25.5		9jan1977	− 18		6jan1942	− 21		22feb1985	− 21
	9dec1927	− 24		9jan1989	− 24		7feb1896	− 18		22jan1911	− 19.5
	9feb1887	− 25.5		10jan1909	− 19.5		10feb1896	− 19.5		22jan1925	− 18
	10jan1935	− 16.5		10jan1977	− 21		11jan1990	− 19.5		23feb1985	− 31.5
	11jan1935	− 18		11jan1977	− 19.5		12jan1990	− 19.5		24jan1925	− 22.5
	11jan1964	− 21		13feb2005	− 21		14jan1964	− 21		25dec1931	− 22.5
	11mar1992	− 24		13jan1910	− 27		15jan1950	− 21		25jan1925	− 27
	12jan1964	− 19.5		14feb2005	− 24		15jan1993	− 27		26jan1887	− 27
	12jan2009	− 22.5		14jan1885	− 22.5		16feb1950	− 24		26jan1925	− 31.5
	12mar1992	− 25.5		14jan1910	− 22.5		16jan1950	− 33		27jan1887	− 31.5
	13jan1901	− 15		15feb2005	− 22.5		17jan1950	− 31.5		27jan1992	− 23.5
	14feb1911	− 34.5		14jan2008	− 22.5		18feb1950	− 21		28jan1911	− 21
	15feb1911	− 28.5		15jan1910	− 22.5		18jan1993	− 16.5		28jan1950	− 19.5
	16feb1887	− 24		15jan1954	− 29		19jan1993	− 22.5		29dec1924	− 21
	16jan2006	− 21		15jan2008	− 24		20feb1959	− 16.5		29jan1911	− 30
	19jan1898	− 27		16jan1910	− 22.5		21feb1959	− 25.5		30jan1887	− 22.5
	18jan2008	− 15		16jan1954	− 25.5		22feb1959	− 19.5		30jan1974	− 22.5
	20jan1925	− 18		17feb1927	− 24		22jan1957	− 24		31dec1948	− 21
	20jan1973	− 16.5		17feb1993	− 24		22jan1964	− 24	P5	6dec1994	− 25.5
	21feb1949	− 21		17jan1993	− 27		22jan1993	− 22.5		7feb1950	− 28.5
	22feb1959	− 25.5		18feb1927	− 24		23dec1905	− 27		7jan1885	− 25.5
	20jan1950	− 16.5		18jan1950	− 22.5		23jan1911	− 24		17jan1973	− 21
	23feb1897	− 16.5		18jan1954	− 21		23jan1964	− 25.5		18jan1973	− 25.5
	24jan1964	− 25.5		19feb1927	− 21		24dec1905	− 27		19jan1973	− 27
	25dec1972	− 24		20feb1994	− 18		24jan1911	− 27	P6	7dec1994	− 28.5
	27jan1925	− 34.5		20jan1973	− 16.5		25jan1964	− 22.5		8dec1994	− 24
	27jan1992	− 22		20jan1984	− 15		26dec1931	− 22.5		25jan1911	− 27
	28jan1992	− 24		22jan1890	− 22.5		27dec1931	− 16.5		27jan1983	− 21
	29jan1896	− 19.5		22jan1894	− 16.5		27jan1921	− 19.5	P7	30jan1911	− 25.5
	29jan1946	− 18		22jan2006	− 22.5		28dec1905	− 22.5	P8	17jan2006	− 21
	30jan1950	− 19.5		23jan1894	− 22.5		28feb1959	− 21	P9	19jan1950	− 19.5
	31dec1889	− 21		25jan1903	− 21		28jan1925	− 28.5		19feb1950	− 24
	31jan1876	− 21		27dec2002	− 34.5		28jan1983	− 21	P10	26dec2002	− 31.5

Acknowledgements The authors would like to thank NOAA and the Iranian Meteorological Organization for providing access to the upper air data and that from the Tabriz station, and from Dr. Azra Khosravi Chenar for her help in providing the high-quality maps. The authors acknowledge the role of the anonymous reviewer and the editor in chief who helped to make this work stronger.

Author contribution MA: conceptualization, methodology, investigation, analysis, writing the original manuscript; ARL: conceptualization, analysis, writing, reviewing, editing; YGHR: conceptualization, data collection, coding, reviewing; BS: reviewing; MFA: reviewing.

Availability of data and material The datasets generated during the current study are available from the corresponding author on reasonable request.

Code availability Code is available from the author upon request.

Declarations

Ethics approval The authors paid attention to the ethical rules in the study. There is no violation of ethics.

Consent to participate The manuscript has been read and approved by all named authors, and there are no other people who satisfied the criteria for authorship but are not listed. The order of authors listed in the manuscript has been approved by all the authors.

Consent for publication The authors transfer to Springer the nonexclusive publication rights. The transfer of publication rights covers the non-exclusive rights to reproduce and distribute the article including reprints, translations, photographic reproductions, electric forms (online, offline), or any other reproductions of similar nature.

Conflict of interest The authors declare no competing interests.

References

Aalijahan M, Khosravichenar A (2021) A multimethod analysis for average annual precipitation mapping in the Khorasan Razavi Province (Northeastern Iran). Atmosphere 12(5):592

Aalijahan M, Salahi B, Rahimi YG, Asl MF (2019) A new approach in temporal-spatial reconstruction and synoptic analysis of cold waves in the northwest of Iran. Theoret Appl Climatol 137(1):341–352

Abatan AA, Abiodun BJ, Lawal KA, Gutowski WJ (2016) Trends in extreme temperature over Nigeria from percentile-based threshold indices. Int J Climatol 36(6):2527–2540

Abbas F, Sarwar N, Ibrahim M, Adrees M, Ali S, Saleem F, Hammad HM (2018) Patterns of climate extremes in the coastal and highland regions of Balochistan. Pakistan Earth Interactions 22(6):1–23

Abrahams AD (1972) Factor analysis of drainage basin properties: evidence for stream abstraction accompanying the degradation of relief. Water Resour Res 8(3):624–633

Aguilar, E., Peterson, T. C., Obando, P. R., Frutos, R., Retana, J. A., Solera, M., ... & Valle, V. E. (2005). Changes in precipitation and temperature extremes in Central America and northern South America, 1961–2003. Journal of Geophysical Research: Atmospheres, 110(D23).

Ahmadi M, Ghavidel-Rahimi Y (2011) Identification and analysis of low temperatures in the northwestern region of Iran using NTD method. Journal of Earth Science Research 2(6):77–94

Alexander, L. V., Zhang, X., Peterson, T. C., Caesar, J., Gleason, B., Tank, A. K., ... & Tagipour, A. (2006). Global observed changes in daily climate extremes of temperature and precipitation. Journal of Geophysical Research: Atmospheres, 111(D5).

Alijani B, Houshyar M (2008) Identification of synoptic patterns of severe colds in the northwest of Iran. Physical Geography Research Quarterly 65:1–16

Alijani B (2009) Synoptic climate, 3rd edn. Samt Publication, Tehran, Iran

Anagnostopoulou C, Tolika K, Lazoglou G, Maheras P (2017) The exceptionally cold january of 2017 over the Balkan Peninsula: a climatological and synoptic analysis. Atmosphere 8(12):252

Bartzokas A, Metaxas DA (1995) Factor analysis of some climatological elements in Athens, 1931–1992: covariability and climatic change. Theoret Appl Climatol 52(3–4):195–205

Beniston M, Stephenson DB, Christensen OB, Ferro CA, Frei C, Goyette S, ... & Palutikof J (2007). Future extreme events in European climate: an exploration of regional climate model projections. Climatic change, 81(1), 71-95

Brown, S. J., Caesar, J., & Ferro, C. A. (2008). Global changes in extreme daily temperature since 1950. Journal of Geophysical Research: Atmospheres, 113(D5).

Cassano EN, Lynch AH, Cassano JJ, Koslow MR (2005) Classification of synoptic patterns in the western Arctic associated with extreme events at Barrow, Alaska, USA. Climate Res 30(2):83

Compo GP, Sardeshmukh PD, Whitaker JS, Brohan P, Jones PD, McColl C (2013) Independent confirmation of global land warming without the use of station temperatures. Geophys Res Lett 40(12):3170–3174

Cattiaux J, Yiou P, Vautard R (2012) Dynamics of future seasonal temperature trends and extremes in Europe: a multi-model analysis from CMIP3. Clim Dyn 38(9–10):1949–1964

Ceccherini G, Russo S, Ameztoy I, Romero CP, Carmona-Moreno C (2015) Magnitude and frequency of heat and cold waves in recent decades: the case of South America. Nat. Hazards Earth Syst. Sci. Discuss. 3:7379–7409

Cheng X, Nitsche G, Wallace JM (1995) Robustness of low-frequency circulation patterns derived from EOF and rotated EOF analyses. J Clim 8(6):1709–1713

Cony M, Hernández E, Del Teso T (2008) Influence of synoptic scale in the generation of extremely cold days in Europe. Atmósfera 21(4):389–401

Cony ME, Del Teso Hernandez T (2008) Influence of synoptic scale in the generation of extremely cold days in Europe. Atmosfera 21:389–401

Cooney, C. M. (2012). Managing the risks of extreme weather: IPCC Special Report.

Della-Marta, P. M., Haylock, M. R., Luterbacher, J., & Wanner, H. (2007). Doubled length of western European summer heat waves since 1880. Journal of Geophysical Research: Atmospheres, 112(D15).

Della-Marta PM, Luterbacher J, von Weissenfluh H, Xoplaki E, Brunet M, Wanner H (2007b) Summer heat waves over western Europe 1880–2003, their relationship to large-scale forcings and predictability. Clim Dyn 29(2–3):251–275

Domonkos P, Kysely J, Piotrowicz K, Petrovic P, Likso T (2003) Variability of extreme temperature events in south-central Europe during the 20th century and its relationship with large-scale circulation. Int J Climatol 23(9):987–1010

Dutta S, Chaudhuri G (2015) Evaluating environmental sensitivity of arid and semiarid regions in northeastern Rajasthan. India Geographical Review 105(4):441–461

Easterling DR, Meehl GA, Parmesan C, Changnon SA, Karl TR, Mearns LO (2000) Climate extremes: observations, modeling, and impacts science 289(5487):2068–2074

Efe B, Sezen İ, Lupo AR, Deniz A (2020) The relationship between atmospheric blocking and temperature anomalies in Turkey between 1977 and 2016. Int J Climatol 40(2):1022–1037

Farajzadeh M (2007) Climatological techniques, 1st edn. Samt Publication, Tehran, Iran

Feoktistov VM, Kharin VN, Specktor EN (2007) Hierarchical factor analysis applied for interpreting chemical elements deposited with atmospheric precipitation in Karelia. Russ Meteorol Hydrol 32(12):761–769

Founda D, Giannakopoulos C (2009) The exceptionally hot summer of 2007 in Athens, Greece—a typical summer in the future climate? Global Planet Change 67(3–4):227–236

Gao M, Franzke CL (2017) Quantile regression–based spatiotemporal analysis of extreme temperature change in China. J Clim 30(24):9897–9914

Ghasemi AR (2015) Changes and trends in maximum, minimum and mean temperature series in Iran. Atmospheric Science Letters 16(3):366–372

GhavidelRahimi Y (2011) Determination of statistical threshold and synoptic analysis of cold temperatures in Maragheh. Journal of Applied Geosciences Research 19(22):62–45

GhavidelRahimi Y (2011) The relationship between the low extreme temperatures of cold period of Azerbaijan with 500 hPa of circulation patterns. Journal of Geographic Space 11(35):183–155

Ghavidel-Rahimi Y, Farajzadeh-Asl M, Motallbeiizadeh S (2016) Statistical and synoptic analysis of cold waves in the northwest region of Iran. Journal of Applied Researches in Geographical Sciences 16(40):29–46

Ghavidel-Rahimi Y. (2009) Synoptic analysis of extreme temperatures in the northwest of Iran during the cold season, PhD thesis, Faculty of Literature and Humanities, Physical Geography Department, Isfahan University, Iran.

Golden JS, Hartz D, Brazel A, Luber G, Phelan P (2008) A biometeorology study of climate and heat-related morbidity in Phoenix from 2001 to 2006. Int J Biometeorol 52(6):471–480

Hankes, I. E., & Walsh, J. E. (2011). Characteristics of extreme cold air masses over the North American sub-Arctic. Journal of Geophysical Research: Atmospheres, 116(D11).

Hann, C. T. 1986. Statistical Methods in Hydrology, IOWA State University Press/Ames.

Harsant J, Pavlovic L, Chiu G, Sultmanis S, Sage TL (2013) High temperature stress and its effect on pollen development and morphological components of harvest index in the C3 model grass Brachypodium distachyon. J Exp Bot 64(10):2971–2983

Hervada-Sala C, Eusebi JB (2004) A program to perform Ward's clustering method on several regionalized variables. Computers & Geosciences 30(8):881–886

Horton DE, Johnson NC, Singh D, Swain DL, Rajaratnam B, Diffenbaugh NS (2015) Contribution of changes in atmospheric circulation patterns to extreme temperature trends. Nature 522(7557):465

Kebede AS, Dunford R, Mokrech M, Audsley E, Harrison PA, Holman IP, ... & Sallaba F (2015). Direct and indirect impacts of climate and socio-economic change in Europe: a sensitivity analysis for key land-and water-based sectors. Climatic change, 128(3-4), 261-277.

Kyselý J (2008) Influence of the persistence of circulation patterns on warm and cold temperature anomalies in Europe. Analysis over the 20th Century. Global Planet Change 62:147–163

Lashkari H (2008) Synoptic analysis of cold wave 2003 in Iran. Geographical Research 40(66):1–18

López-Díaz F, Conde C (2013) Analysis of indices of extreme temperature events at Apizaco, Tlaxcala, Mexico: 1952–2003. Atmósfera 26(3):349–358

Lupo AR, Nocera JJ, Bosart LF, Hoffman EG, Knight DJ (2001) South American cold surges: types, composites, and case studies. Mon Weather Rev 129(5):1021–1041

Masoudian A, Darand M (2011) Synoptic analysis of extreme temperatures in Iran. Geography and Development 22:165–185

Matiu M, Ankerst DP, Menzel A (2016) Asymmetric trends in seasonal temperature variability in instrumental records from ten stations in Switzerland, Germany and the UK from 1864 to 2012. Int J Climatol 36(1):13–27

Mayowa OO, Pour SH, Shahid S, Mohsenipour M, Harun SB, Heryansyah A, Ismail T (2015) Trends in rainfall and rainfall-related extremes in the east coast of peninsular Malaysia. J Earth Syst Sci 124(8):1609–1622

Meehl GA, Tebaldi C (2004) More intense, more frequent, and longer lasting heat waves in the 21st century. Science 305(5686):994–997

Mika J (2013) Changes in weather and climate extremes: phenomenology and empirical approaches. Clim Change 121(1):15–26

Mo D, Hou Y, Li J, Liu Y (2016) Study on the storm surges induced by cold waves in the Northern East China Sea. J Mar Syst 160:26–39

Mohan S, Arumugam N (1996) Relative importance of meteorological variables in evapotranspiration: factor analysis approach. Water Resour Manage 10(1):1–20

Monier E, Gao X (2015) Climate change impacts on extreme events in the United States: an uncertainty analysis. Clim Change 131(1):67–81

Nadi M, Khalili A (2013) Climatological Classification of precipitation in Iran by clustering-factor analysis. Journal of Water and Soil 44(3):222–244

Nunes MJ, Lupo AR, Lebedeva MG, Chendev YG, Solovyov AB (2017) The occurrence of extreme monthly temperatures and precipitation in two global regions. Papers in Applied Geography 3(2):143–156

Najafi A, Nasri M (2009) Affecting factors of flood in basin of Isfahan - Sirjan by factor analysis. Journal of Geography and Environmental Planning 36(4):101–118

Ning L, Bradley RS (2015) Winter climate extremes over the northeastern United States and southeastern Canada and teleconnections with large-scale modes of climate variability. J Clim 28(6):2475–2493

Pachauri, R. K., Allen, M. R., Barros, V. R., Broome, J., Cramer, W., Christ, R., ... & Dubash, N. K. (2014). Climate change 2014: synthesis report. Contribution of Working Groups I, II and III to the fifth assessment report of the Intergovernmental Panel on Climate Change (p. 151). IPCC.

Parey S, Hoang TTH (2015) Changes in the distribution of cold waves in France in the middle and end of the 21st century with IPSL-CM5 and CNRM-CM5 models. Climate Dynamic. https://doi.org/10.1007/s00382-015-2877-6

Peterson, Thomas C and et al. (2013). Monitoring and understanding changes in heat waves, cold waves, floods and droughts in the United States. Bulletin of the American Meteorological Society. 821–834.

Prieto L, Garcia R, Diaz J, Hernandez E, Del Teso T (2002) NAO influence on the extreme winter temperature in Madrid (Spain). Annals Geophysical 20:2077–2085

Prieto L, Herrera RG, Díaz J, Hernández E, del Teso T (2004) Minimum extreme temperatures over Peninsular Spain. Global Planet Change 44(1):59–71

Radinović D, Ćurić M (2012) Criteria for heat and cold wave duration indexes. Theor Appl Climatol 107:505–510

Ryoo SB, Kwon KB, Jhun JG (2005) Surface and upper-level features associated with wintertime cold surge outbreaks in South Korea. Adv Atmos Sci 22:509–524

Salguero-Gómez R, Siewert W, Casper BB, Tielbörger K (2012) A demographic approach to study effects of climate change in desert plants. Philosophical Transactions of the Royal Society b: Biological Sciences 367(1606):3100–3114

Schindler DW (1997) Widespread effects of climatic warming on freshwater ecosystems in North America. Hydrol Process 11(8):1043–1067

Shahid S (2010) Recent trends in the climate of Bangladesh. Climate Res 42(3):185–193

Simmonds I, Richter T (2000) Synoptic comparison of cold events in winter and summerin Melbourne and Perth. Theoretical and applied climatology 67(1–2):19–32

Song C, Pei T, Zhou C (2014) The role of changing multiscale temperature variability in extreme temperature events on the eastern and central Tibetan Plateau during 1960–2008. Int J Climatol 34(14):3683–3701

Takahashi H (1990) Migration of the cold air mass related to rain belt formation of the Chinese continent and atmospheric systems during the Baiu Season (In apanese). Geographical Review of Japan; Series A 64:10–24

Tannehill IR (1928) Severe cold waves on the Texas coast. Monthly Weather Review 56(2):41–47

Unkašević M, Tošić I (2015) Seasonal analysis of cold and heat waves in Serbia during the period 1949–2012. Theoret Appl Climatol 120(1–2):29–40

Van Oldenborgh GJ, Haarsma R, De Vries H, Allen MR (2015) Cold extremes in North America vs. mild weather in Europe: the winter of 2013–14 in the context of a warming world. Bulletin of the American Meteorological Society 96(5):707–714

Whan K, Zwiers F, Sillmann J (2016) The influence of atmospheric blocking on extreme winter minimum temperatures in North America. J Clim 29(12):4361–4381

White EL (1975) Factor analysis of drainage basin properties: classification of flood behavior in terms of basin geomorphology. Water Resour Bull 11(4):676–687

You Q, Kang S, Aguilar E, Pepin N, Flügel WA, Yan Y, ... & Huang J (2011). Changes in daily climate extremes in China and their connection to the large scale atmospheric circulation during 1961–2003. Climate Dynamics, 36(11-12), 2399-2417

Zhang, Kenneth R. Sperber and James S. Boyle, 1996. Climatology of East Asian winter monsoon and cold surges, PCMDI Report 38.